

Dose Response Modeling for Targeted Radiotherapies

PL Roberson, PhD
Department of Radiation Oncology
University of Michigan

Targeted radiotherapies (TRT) offer a systemic treatment with a therapeutic advantage using a carrier designed to attach to a targeted tissue (i.e. tumor). Below, TRTs are introduced; challenges of identifying dose-response correlations are described; tissue response modeling is described; and finally two examples of the use of response models are presented.

What are Targeted Therapies?

The efficacy of biologically targeted radionuclide therapy is dependent on the properties of the treatment strategy, the carrier (or vector, see Table 1), the radionuclide products, and the target and normal tissue architecture. Important properties of the carrier are biospecificity, in-vivo stability, target type and carrier-target affinity, carrier distribution in target and non-target sites, and interaction with tissue microenvironment.

Table 1. Example Carriers

Carrier Type	Example	Molecular Weight or size	Target
Monoclonal Antibody	IgG2a	~150 kDa	cell antigen
Antibody fragment	Fab	50-100 kDa	cell antigen
Peptide	DOTATOC	~1 kD	somatostatin receptor
Small molecule	mIBG	~0.3 kD	adrenergic tissue
Microsphere	Glass or plastic spheres	~25 um	liver tumor capillaries
Bispecific (multi-step)	Tri-Fab + hapten-peptide	~100kDa + ~1 kD	cell antigen

For the purpose of delivering absorbed dose to the target tissue, a radionuclide is attached to the carrier. Table 2 lists popular radioisotopes for targeted therapies. Beta emitters have the advantage of being able to inactivate a cell at a distance, depending on the ranges of the beta particles. Alpha particles and Auger electrons target locally, but have a much greater damage potential per decay (relative biological Effect (RBE)) \gg 1). For optimum therapeutic ratio, the radionuclide half-life should be matched to the carrier residence times in the target and normal tissues.

Table 2. Popular Radionuclides and their Properties

Radionuclide	Therapeutic Radiation	Average Energy	Half-Life
Y-90	Beta	940 keV	64 hr
I-131	Beta	180 keV	8.0 d
Lu-177	beta	130 keV	6.7 d
At-211	Alpha	6.8 MeV	7.2 hr
In-111	Auger electron	5 to 25 eV	3 d

Example TRTs matching targeted diseases with carrier and isotope are given in Table 3.¹

Table 3. Examples Targeted Radiotherapies

Site Category	Targeted Disease	Carrier	Isotope	Example
Hematological	Non-Hodgkin's Lymphoma	Anti-CD20 IgG2a	I-131	I131-Tositumomab (BEXXAR)
		Anti-CD20 IgG1	Y-90	Ibritumomab tiuxetan (ZEVALIN)
Neuroectoderm	Neuroblastoma	Meta-iodobenzylguanidine (mIBG)	I-131	mIBG
Neuroendocrine	Gastro-Entero-Pancreatic (GEP)	Peptide	In-111 Y-90	In111-Octreotide Y90- DOTATOC Lu177-DOTATATE
Liver	Hepatocellular Carcinoma	Microspheres	Y-90	Theraspheres

“Dose” Response of Targeted Therapies

Standard methods for the calculation of dose are specified by the Committee on Medical Internal Radiation Dose (MIRD).² Historically, these are based on radionuclide (activity) residence times, radiation properties, and standard source and target geometries. S values are precalculated values representing the average dose (D) to a target organ from a source organ with unit uniform cumulated activity (A): $D = A \times S$. Alternatively, source and target regions can be subdivided for improved definition of source region and specificity of tissue response. See MIRD 19³ for an example of standard kidney models with substructures specified. With the advent of 3D imaging using SPECT/CT and/or PET/CT, fully 3D voxel dosimetry or hybrid methods are also possible.⁴

Both dose estimation and cellular response for TRTs are more complex than typical external beam therapy or sealed source brachytherapy, for both targeted and normal tissues. Estimation of targeted therapy dose response of normal and target tissues suffers from inaccurate macroscopic dose estimation, heterogeneous microscopic dose and dose rate dependence, and confounding factors including pretreatment patient status and treatment synergy with concurrent treatment regimens.

Significant target changes during therapy are due to typically longer therapeutic intervals and the microscopic structure of targeted tissues. Macro vs Micro distributions of sensitive target tissues and carrier uptake distributions vary in significance because of differing penetrating ability of the radiations.

Tissue response depends on component cell survival, being influenced by apoptosis, damage repair, division delay, cell cycle redistribution, reoxygenation, and regeneration. Tissue response to radiation damage has been quantified according to damage to cellular and intercellular structures. Radiation exposure creates damage to the cellular DNA, cellular structure and interstitial structures that affect function. A dose of 1 Gy of low linear-energy transfer (LET) radiation creates approximately 800 single strand breaks (SSBs), 40 double strand breaks (DSBs), and other extensive damage to the DNA structure.⁵ Therapy success within normal tissue tolerances have been related to cell death resulting in tumor shrinkage and normal tissue function disruption. Cell death is directly related to distinct pathways of prompt apoptosis, autophagy, senescence, catastrophic death and delayed apoptosis.⁶

The process of tumor control or normal tissue damage is complex. Gross tissue response is related to the viability of its component cells. Normal, controlled cell death can be accomplished with apoptosis, senescence or autophagy. If a cell detects damage, it can trigger its own death via a controlled pathway. If many cells are damaged in a tissue, signals are sent out triggering increased cellular repair (a bystander effect) in an effort to save the tissue. House-keeping genes send signals to hold up the cell cycle and make repairs or eliminate damaged cells by apoptosis. Increased cell damage after repair signaling can cause catastrophic (mitotic) cell death with an associated inflammatory tissue response. Tissue changes due to significant cell death can alter tissue oxygenation status (reoxygenation) and trigger accelerated repopulation and redistribution in the cell cycle.

Despite the challenges of performing accurate dose calculations and the large variations in dose rates, some correlations between tissue response and dose have been observed for targeted therapies. Brans et al.⁷ reviewed the search for a dose response (“the quest for the “Holy Gray”) and concluded that the biological effect (“BEGray”) is a more appropriate object of a quest. Stabin⁸ reviewed the evidence for dose response and emphasized the need for patient-specific dosimetry.

Evidence for dose response for bone marrow has been mixed. Platelet toxicity grade did not correlate with red marrow dose for Y90 Zevalin, where the calculation used reference adult geometry.⁹ This may not be surprising considering the patient population is relapsed or refractory non-Hodgkin's lymphoma, where significant prior cytotoxic therapies and some variable marrow targeting is the norm. A positive correlation of marrow toxicity with marrow dose was reported by Shen et al.¹⁰ for a non-marrow targeting Y90 (anti TAG-72) antibody therapy. They used CT-based patient-specific marrow mass and an estimation of total marrow mass from measurements in three lumbar vertebrae. Image-based estimates of dose to red marrow are more reliable than blood-based estimates.

Average organ dose calculations with standard reference organ geometries generally do not show correlation of tissue response with dose and are not adequate for therapy planning. For treatments of neuroendocrine tumors with radiolabeled peptides (DOTATOC), a significant correlation between tumor shrinkage at the end of therapy and tumor dose was found. There was also a positive correlation between platelet reduction and red marrow dose. Even with these successes in demonstrating a dose correlation, the general principle of dose response is yet to be confirmed under all conditions for peptide therapies.¹¹

The demand for improved dose (or therapy)-response modeling, a prerequisite for improved therapy dose optimization, requires more extensive and detailed knowledge of a (potentially) dynamic activity distribution and of tissue status (e.g cell repair potential, proliferation potential, etc.) Needed information can be gained by SPECT and PET imaging. Effects that require detailed imaging are: 1) target changes over extended therapy intervals; 2) volumes and microscopic structures of targeted and normal tissues; and 3) activity uptake distributions over extended intervals. To accomplish this, efforts are being made to perform more frequent high-resolution scanning using dual-energy CT, PET/CT, and SPECT/CT. In addition, micro versus macro distributions of activity has been investigated. Results point to a non-uniform micro structure and/or activity distribution that can be used to modify dose-response estimates based on routine macro distribution measurements.^{12,13} Examples of the need for improved patient-specific imaging include 1) evidence that imaging-based bone marrow doses correlate with outcome better than blood-based methods; 2) dose estimations from 3D (SPECT/CT) methods are significantly superior to 1D (planar) methods; 3) evidence that factors other than dose affect therapy outcomes, possibly with synergistic relationships with dose; 4) considerable range in bio-kinetics present between patients.

Below, the dose, biological dose and therapy effect model equations are presented in the form of the linear-quadratic model and associated enhancements. Two example applications follow: 1) Biological effect model of kidney response and 2) Therapy effect model for non-Hodgkin's lymphoma.

Therapy-Response Modeling

Most significant therapy effects can be described using the **Linear-Quadratic (L-Q) Model**¹⁴, with possible modifications to include apoptosis, cell cycle delay, bystander effects, dose-rate dependent cell cycle (proliferation) delay, oxygenation status, and accelerated proliferative regeneration.

Theoretically, the linear-quadratic model relies on the increasing difficulty of performing cell repair when the number of DSBs is greater than one in specific sensitive DNA domains, although any non-repairable damage relying on one or more than one hit is consistent with the fundamental model. The model assumptions depend on catastrophic (mitotic) cell death as the main avenue to tissue damage. The linear term relates to irreparable single event damage, such as one DNA double strand break. If a second event occurs in close proximity to an earlier repairable event before cellular repairs have been performed, repairable damage can be transformed to irreparable damage. This implies a quadratic dose-response term. The description below will cover several model enhancements to the fundamental L-Q model to account for other phenomena such as high-LET and low dose-rate radiation.

The double hit model implies that dose alone correlates poorly with tissue response unless many exposure parameters are held constant, such as radiation type, dose rate, tissue type, etc. A more appropriate therapy effect calculation uses the Biological Effective Dose (BED), which in its simplest form can be viewed as a biological correction to the absorbed dose,¹⁵

$$BED(r, t) = D(r, t) * RE(r, t)$$

$$RE(r, t) = 1 + \frac{G(r, t)}{\left(\frac{\alpha}{\beta}\right)} * D(r, t)$$

where α and β are the linear and quadratic radiosensitivity coefficients, and the detailed dependence on dose and dose rate are put into $G(r, t)$, the Lea-Catcheside factor. Explicit dependence on space and time recognize the variable dose rates characteristic of TRT.

The L-Q model is fundamentally a cell survival model. The biological effect, E , is related to fractional cell survival (S),

$$E = -\ln(S)$$

Where

$$S = \int \exp[-BED(r, t)] d^3 r dt$$

For a time-dependent dose rate at a time t post therapy initiation,¹⁶

$$G(r, t) = \left[\frac{2}{D(r, t)^2} \right] \int_0^t \dot{D}(r, t') dt' \int_0^{t'} \dot{D}(r, w) e^{-\mu(t'-w)} dw$$

Where $\dot{D}(r, t)$ is the dose rate and μ is the repair coefficient equal to $\ln(2)$ divided by the half-time for repair. This formula keeps track of the time interval between events and alters the probability of successful repair based on the repair half-time. For a single (instantaneous) fraction, $G=1$, yielding the standard formula applied for most external beam therapies.

Targeted therapies typically experience both radioactive and biological clearance, described as effective decay. For a continuously decaying source with effective decay constant λ ,

$$\dot{D}(t) = \dot{D}_0 e^{-\lambda t}$$

and

$$G = \lambda / (\lambda + \mu)$$

So that,

$$BED = D * \left[1 + \frac{D}{\left(\frac{\alpha}{\beta}\right)} * \left(\frac{\lambda}{(\lambda + \mu)}\right) \right]$$

A voxelized description replaces the spatial dependence of the quantities by values for each voxel (ijk),¹⁷

$$BED^{ijk} = D^{ijk} + \frac{\beta * D^{ijk}}{\alpha} * \left(\frac{\lambda^{ijk}}{\lambda^{ijk} + \mu}\right)$$

where the damage repair rate is constant, but the decay rate is spatially varying because it represents combined radiological decay and variable biological clearance. For easier comparison between therapy types, the BED can be used to estimate a uniform dose that would achieve the same biological effect (Equivalent Uniform Dose, EUD),

$$EUD = -\frac{1}{\alpha} \ln \left(\frac{1}{V} \sum_{ijk} e^{-\alpha \cdot BED^{ijk}} \right)$$

where V is the sum of all voxels (i.e volume). Note that this formula represents a uniform dose delivered at a low dose rate limit, removing the effect of the dose-dependent

quadratic term. Alternatively, summary descriptions can be derived from the voxelized description to form volume histograms for BED (BVHs). The BVHs can be normalized and converted to probabilistic functions, $P(\psi)$, where ψ takes on all values of BED. Then,¹⁸

$$EUD = -\frac{1}{\alpha} \ln \left(\int_0^{\infty} P(\psi) e^{-\alpha\psi} d\psi \right)$$

Non-dose term(s) and cell proliferation can be included into the biologic effect,¹⁵

$$E = -\ln \left(\frac{1}{V} \sum_{ijk} e^{-\alpha \cdot BED^{ijk} - F^{ijk} + \gamma \cdot t} \right)$$

where F^{ijk} represents the non-dose effect(s) and γ is the cell proliferation constant. γ is equal to $\ln(2)$ divided by the effective potential doubling time, T_{pot} . In some publications, the BED includes the proliferation term. Equivalently, similar formulas can be written for the probabilistic and space-time descriptions.

Only α is modified for radio-sensitivity changes, necessary for hyper-radiosensitivity (HRS) effects and for high-LET radiation. For high-LET radiation, radiosensitivity changes are described by the relative biological effect (RBE), such as in alpha particle or Auger electron therapies,¹⁹

$$\alpha = \alpha_r * RBE \quad (\text{high LET})$$

where α_r is the radiosensitivity coefficient typically applied for low-LET radiation with active cell repair.

HRS introduces a competing mechanism (e.g. apoptosis) for cell death resulting in a dose and dose-rate dependence of radiosensitivity.²⁰⁻²² HRS can be represented by a modification of α , which is now space and time dependent,

$$\alpha(r,t) = \alpha_r [1 + (\omega - 1)A(r,t)] \quad (\text{HRS})$$

$$A(r,t) = e^{-\left(\frac{D(r,t)}{D_c} + I\right)}$$

where α_r is the radiosensitivity after repair is turned on (the familiar α of external beam therapies), and ω (~ 3) is the radiosensitivity enhancement factor at low doses. $A(t)$ represents the transition of turning on cell repair, characterized by a critical dose, $D_c \sim 0.3$ Gy and previous cellular insult, I , possibly due to prior treatment. When cell repair is activated, cell cycling is stopped while awaiting cell repair. This effect can be incorporated into T_{pot} .

$$T_{pot}(r, t) = T_{pot0} / [A(r, t) + e^{-\frac{D(r, t)}{Dc}} (1 - A(r, t))]$$

Where T_{pot0} is the initial proliferation half-time and Dc (~ 0.017 Gy/hr) is the critical dose rate signaling cell cycle delay.

Example: Biological Effect for Kidney

Renal toxicity from standard fractionated external beam radiotherapy is observed in approximately 5% of patients in 5 years given bilateral whole kidneys doses of 18 Gy.²³ In contrast to the uniform doses given in external beam, renal dose for targeted therapies is typically given at continuous low dose rates with an inhomogeneous distribution and non-uniform dose rate caused by differing radiation types, energies and path lengths. Dose distributions for targeted therapies suffer from a greater degree of uncertainty.²⁴ A comparison of the impact of dose rate and effective clearance rates for targeted therapies is given by Dale.²⁵

Kidney toxicity is the most likely dose limiting toxicity for targeted therapies after bone marrow. Second-organ toxicities may be cardio-pulmonary for higher molecular weight delivery systems (e.g. intact IgG), but are more likely to be renal for lighter molecules. For targeted therapies using low-molecular weight molecules, such as those based on peptides, the kidneys are a primary route of excretion and are known to concentrate certain radiometals. For example, because somastatin receptors are over-expressed in tumors of neuroendocrine origin, light-weight radiolabeled somastatin analogues were developed for targeted therapy (e.g. ^{90}Y -[DOTA]⁰-Tyr3-octreotide, abbreviated ^{90}Y -DOTATOC).²⁶ Compared to other TRTs, the primary organ of toxicity shifted to the kidneys.

Radiotherapy-induced kidney injury (nephrotoxicity) can be subclinical and clinical. Clinical toxicity includes hypertension headache, edema, dyspnea, fatigue, nausea, vomiting, confusion coma and death. Symptoms can arise over timescales ranging from 6 to 12 months for acute and ranging up to many years for chronic radiation nephrotoxicity.²⁴

The route of kidney clearance for molecular conjugates depends on molecular weight (Table 4). Small molecules clear rapidly and predominantly through the glomeruli in the kidney cortex. Activity in the kidney cortex is typically higher than in the medulla. A study performed in mice found that the average activity concentration in the kidney is initially higher but drops faster for the lighter molecules compared to heavier intact antibody molecules (Fig. 1a).²⁷ The intact antibody clears significantly slower. The smaller molecules also have a significantly higher concentration in the cortex than medulla due to filtering in the glomeruli (Fig. 1b).²⁷ Kidney toxicity can be reduced by the use of amino acids.²⁴

Table 4. Kidney clearance of molecular conjugates as a function of molecular weight [from Flynn, et al.²⁷].

Molecular Size	Kidney clearance	Blood clearance	Example
<25 kDa	Cortex (glomeruli)	Rapid	Peptides
60-70 kDa	Filtration inhibited (single valent)		Fab
~100 kDa	High uptake (multivalent)		F(ab) ₂
150 kDa	Slow	Slow	IgG

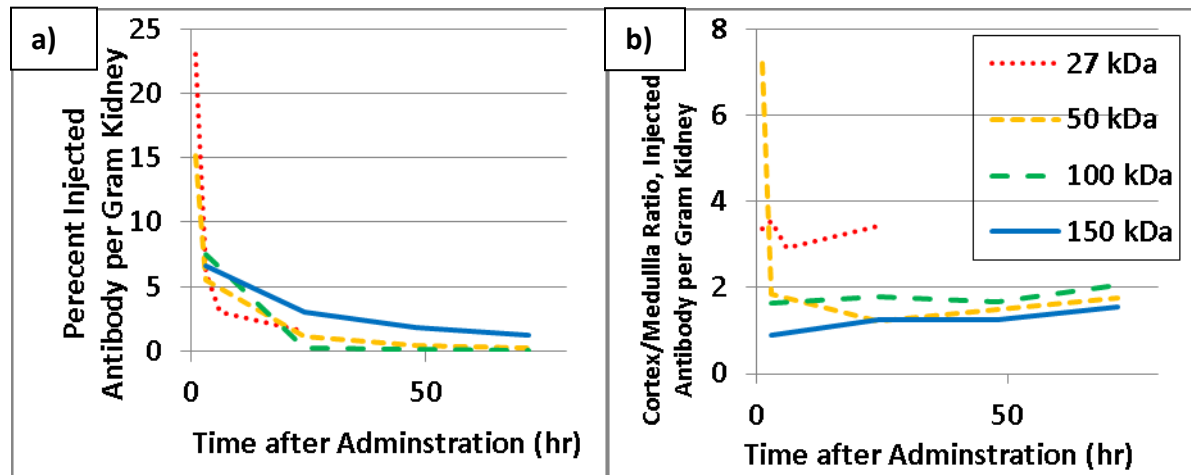


Figure 1. Dependence of Kidney uptake and distribution on molecular weight of carrier. a) Molecular concentration in kidney vs. time post injection; b) Cortex to medulla molecular concentration ratio versus time. Data from Flynn, et al.²⁷

MIRD 19³ presents six age-dependent multi-region kidney models. Barone, et al.²⁸ found that using the S values from MIRD 19 and patient-specific cortex volumes, rather than using S values for standard kidney volumes, improved correlation of the BED with nephrotoxicity. MIRD 20²⁹ makes use of the linear-quadratic model to estimate relative therapy effect by splitting the kidney into two functional subunits (FSUs): the cortex (cor) and medulla (med).

$$S(FSU) = \left(\frac{V_{cor}}{V}\right) e^{-\alpha_{cor}D_{cor} - g(t)\beta_{cor}D_{cor}^2} + \left(\frac{V_{med}}{V}\right) e^{-\alpha_{med}D_{med} - g(t)\beta_{med}D_{med}^2}$$

where $V = V_{cor} + V_{med}$ is the total kidney volume. Dose rate dependence included in $g(t)$ was assumed to have the same functional form for both subunits. From a space and time dependent distribution, the relative therapy effect may be estimated using FSU-dependent

radiosensitivity parameters. Thus, differential distributions of dose rate can be taken into account.

The relationship between absorbed dose to kidney via radionuclide therapies versus external beam therapy is complex. However, morphological and functional features of nephrotoxicity are similar between external beam and targeted therapies.³⁰ Complication rates as a function of dose for radionuclide therapy compared to external beam therapy do not correlate (Fig. 2a). However, when radiobiological corrections are made according to the L-Q model, complication rates are similar (Fig. 2b).

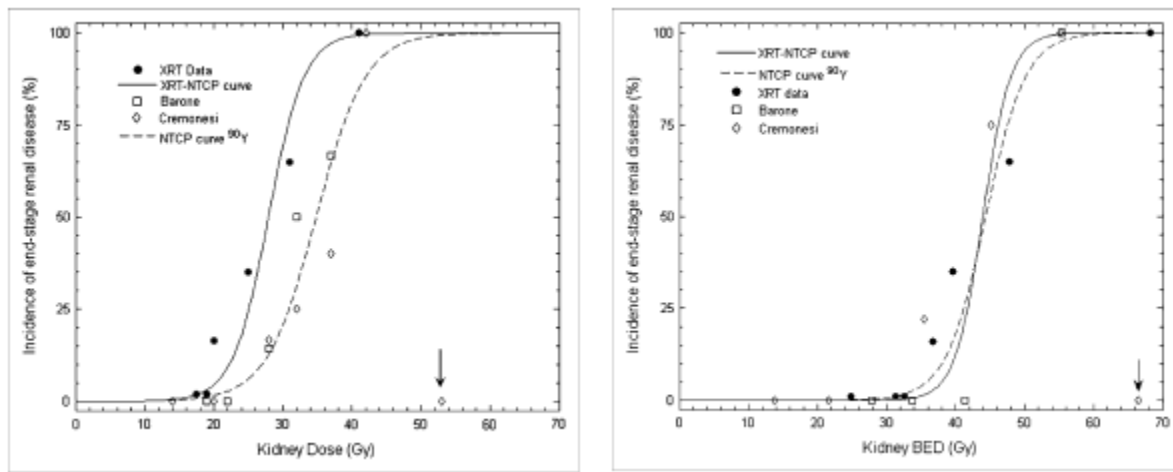


Figure 2. Kidney Response to Dose (a, left panel) and BED (b, right panel). Graphs reproduced from MIRD 20.²⁷ Radionuclide data are for peptide therapy (⁹⁰Y-DOTATOC)[Barone et al.²⁸; Cremonesi, et al.³¹]. External beam data are for standard fractionation [Cassady³²]. Data outlier noted with arrow. For the kidney, half time for repair is 1 to 2 hrs; α/β is 1.5 to 3 Gy.³⁰

The success of the BED concept for peptide therapy is encouraging, but not universal for targeted therapies.²⁹ The failure of other targeted therapy toxicities to correlate with BED estimates may be due to measurement inaccuracies in the time dependence of activity concentrations and associated dose rate distributions and in organ or subunit volumes.

Example: Therapy Effect for Refractory Non-Hodgkin's Lymphoma

There may be a benefit to individualized treatment planning for targeted therapies. This goal may be realized through improved imaging techniques allowing the measurement of molecular uptake distributions as a function of time. Imaging also potentially allows the inclusion of confounding factors, such as the therapeutic response to unlabeled (cold) antibody observed in the treatment of non-Hodgkin's Lymphoma (NHL).

Tositumomab and ¹³¹I-tositumomab (BEXXAR) has successfully treated relapsed or refractory B-cell NHL.³³ Patients receive a tracer infusion (5 mCi) of ¹³¹I-tositumomab followed in 7 or 8

days by a therapeutic infusion (~100 mCi). Both infusions use an initial flood infusion of 450 mg tositumomab followed by a 35 mg infusion tagged with ^{131}I . Patients were imaged 6 times using SPECT/CT, three during the tracer interval and three following the therapeutic infusion. Patients were known to have a significant variation in response to therapy. The variation in response was interpreted as variations in sensitivity to the cold and radiation therapy effects.³⁴ Tumor response to therapy was described using an enhanced L-Q model.³⁵

In the L-Q model, a non-dose term was used, derived from the antibody distributions that were assumed to represent the cold as well as tagged distributions. The non-dose term is

$$\lambda_p \cdot P(r, t)$$

Where

$$P(r, t) = \left(\frac{P_{inj}}{A_{inj} \cdot \rho V} \right) \int_0^t A(r, t') \cdot \exp(\gamma \cdot t') \cdot dt'$$

and λ_p is the cold sensitivity term coefficient, P_{inj} is the injected cold protein, $A(r,t)/A_{inj}$ is the fractional voxel time activity, ρV is the tumor mass, and the exponential term corrects for radioactive decay with decay constant γ . The cold sensitivity parameter is most sensitive to the therapeutic effect observed during the tracer interval and the radiosensitive parameters are most sensitive post therapy infusion. For the HRS model,

$$\lambda_p(r, t) = \lambda_{p0} A(r, t)$$

To relate cell loss to tumor shrinkage, a cell clearance model was required.³⁶ The cell clearance model assumed a linear clearance rate (λ_c), and a further clearance delay for radiation damage (t_d). The additional delay for cell clearance due to radiation damage was needed to fit tumor shrinkage data. It was justified based on the longer time required to clear cell debris after catastrophic mitotic death (and associated inflammation) compared to apoptosis. A change in tumor size (Z) is equal to a negative therapeutic cell loss term (U) and a positive proliferation term,

$$\frac{dZ(t)}{dt} = \frac{dU(t)}{dt} + \gamma \cdot N(t)$$

where

$$\frac{dU(t)}{dt} = -\lambda_c \left[\int_{t_d}^t e^{-\lambda_c \cdot (t-t')} \cdot \alpha \cdot \dot{D}(t' - t_d) \cdot N(t' - t_d) \cdot dt' + \int_0^t e^{-\lambda_c \cdot (t-t')} \cdot \lambda_p \cdot \dot{P}(t') \cdot N(t') \cdot dt' \right]$$

$N(t)$ is the size of remaining cells with proliferative potential. The time-dependent tumor size is

$$Z(t) = Z(0) + \int_0^t \left(\frac{dU(t')}{dt} + \lambda_T \cdot N(t') \right) dt'$$

Measured activity distributions at 6 time points yielded dose rate distributions. The dose rate and activity distributions were connected in time using a radial deformation model resulting in space- and time-dependent descriptions of activity and dose rate.

Initial model fitting was performed using 5 parameters: α , λ_p , λ_c , t_d and $Z(0)$. Proliferation was held constant at $T_{pot} = 150$ d, estimated from time-to-recurrence data. For the majority of tumors, $Z(0)$ differed from unity by less than 10% and was included with the fit to the tracer interval data to reduce the dependence of fit quality on a poorly determined initial tumor volume. Figure 3 shows fits performed for three characteristic tumor responses: no cold sensitivity, high cold sensitivity and high radiosensitivity for constant T_{pot} .

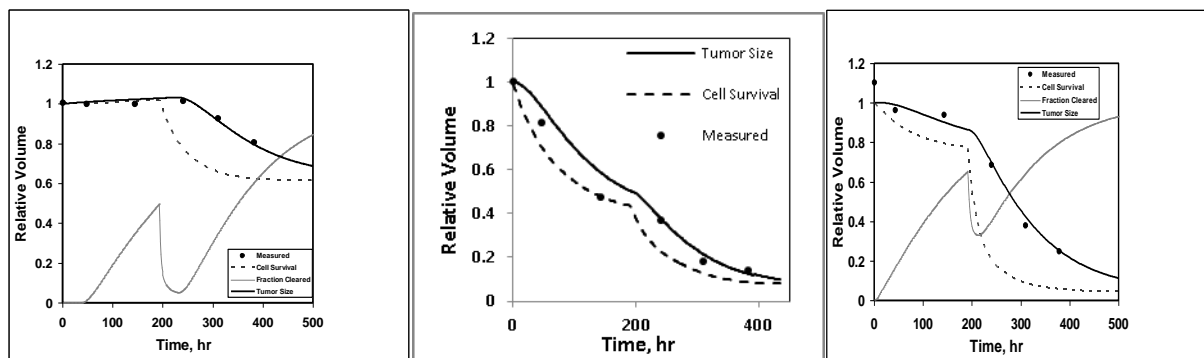


Figure 3. Model fit of tumor shrinkage. Represented are no cold effect (left, $\alpha=0.27 \text{ Gy}^{-1}$, $p=0$), large cold effect (center, $\alpha=0.25 \text{ Gy}^{-1}$, $\lambda_p=0.50 \text{ g}_T/\text{mg}_p/\text{hr}$) and large radio-sensitivity (right, $\alpha=0.95 \text{ Gy}^{-1}$, $\lambda_p=0.02 \text{ g}_T/\text{mg}_p/\text{hr}$). Represented are measured relative tumor volumes (dots), tumor size fit (solid curve), relative cell survival (dotted curve), and fraction of cells cleared (light curve).

Results of the fitting were used to separate the case types into three categories, cases without cold effect, with cold effect and with high radiosensitivity (and cold effect). Averaged parameters from each case category were used to recalculate the EUD and E values. These results were compared to tumor shrinkage observed at 2 months post therapy. The 2-month shrinkage did not correlate with dose or EUD, but did correlate with E (Fig. 4). An important element was the observed large variation of tumor radiosensitivity and cold antibody sensitivity. Dose did not correlate because dose alone ignored the large therapeutic effect of cold antibody. EUD did not correlate because of the large range of radiosensitivity, even though dose rate effects and the cold effect was included. This was interpreted as a validation of the use of a therapy score quantity (E) where dose is only one of several important elements.

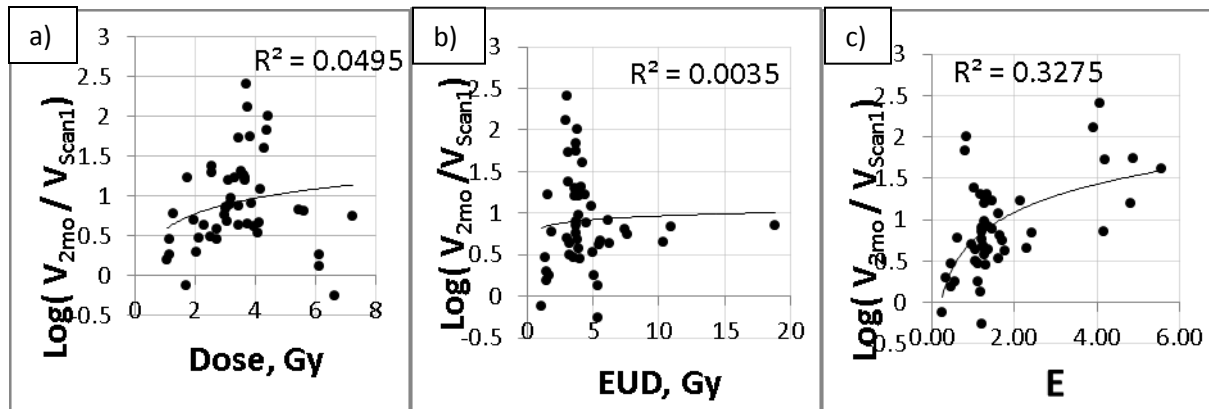


Figure 4. Two-month Tumor Shrinkage correlation with a) Dose, b) EUD and c) E.

HRS vs L-Q

Proliferation was included in the fit by using the 2-month data in a least-square analysis. The least square analysis produced an excellent fit, illustrated by the high correlation of E vs. the 2-month shrinkage data (Fig 5a). The radiosensitivity parameter also was highly correlated (Fig 5b), but the proliferation parameter was not (Fig. 5c). The HRS Model provides an explanation for the range of radiosensitivity, while also affecting the interaction of cold sensitivity and proliferation. The cell clearance model was altered to allow a time delay for mitotic death, but not for apoptosis generated by radiation damage.

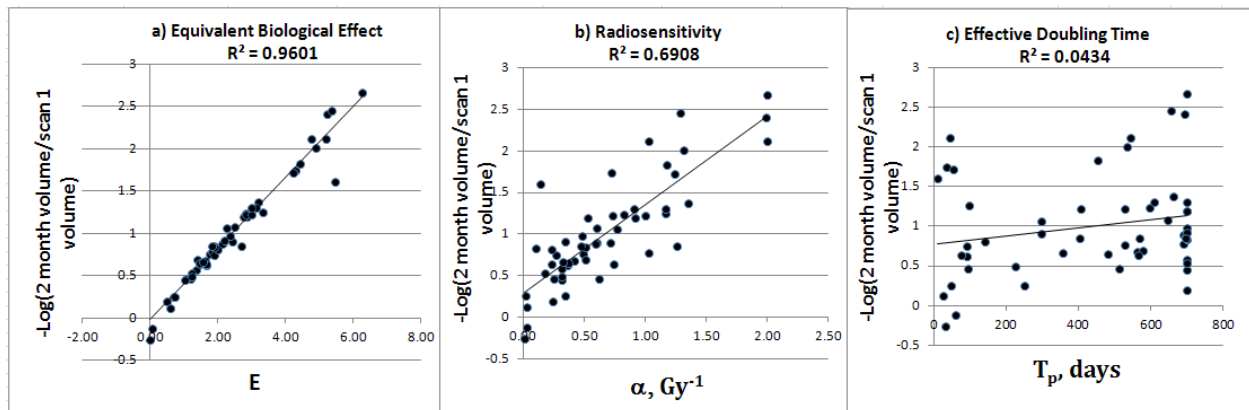


Figure 5. Least squares fit to tumor shrinkage for Non-Hodgkin's Lymphoma treated with ¹³¹I Tositumomab using the Bio-Effect L-Q Model. Correlation of 2- month tumor shrinkage with a) equivalent biological effect (E); b) radio-sensitivity (α); and c) effective doubling time (T_{pot}).

For preliminary work, one tumor from each of 11 patient data sets were chosen for an example fit comparison. The L-Q fit was chosen from initial optimal fits, except in 2 cases where an alternative fit minimum similar to the achievable HRS fit was used. The HRS parameters were adjusted to reproduce a similar fit to tumor shrinkage. The HRS model tended to increase the

effect of the radiosensitivity parameter and decrease the effect of the cold-protein sensitivity parameter. The mean and deviation of the radiosensitivity parameter decreased. There was little change in the mean of the cold sensitivity parameter. The effective doubling time clustered at ~ 700 d for all but one case of obvious high proliferation. HRS modeling decreased the variation between the radiosensitivity and proliferation parameters for these example cases. Improved correlation of mean radiosensitivity and proliferation parameters to outcome is expected.

References

1. W.J.G. Oyen, Bodei, L., Giammarile, F., et al., "Targeted therapy in nuclear medicine - current status and future prospects," *Annals of Oncology* 18 (11), 1782-1792 (2007).
2. R. Loevinger, Budinger, T.F., Watson, E.E., *MIRD Primer for Absorbed Dose Calculations*. (The Society of Nuclear Medicine, New York, 1991).
3. L.G. Bouchet, Bolch, W.E., Blanco, H.P., et al., "MIRD Pamphlet No. 19: Absorbed fractions and radionuclide S values for six age-dependent multiregion models of the kidney," *J Nucl Med* 44 (7), 1113-1147 (2003).
4. G. Sgouros, "Dosimetry of internal emitters," *J Nucl Med* 46 (1), 18S-27S (2005).
5. D. Murray, Weinfeld, M., "Radiation biology of targeted radiotherapy", in *Monoclonal Antibody and Peptide-Targeted Radiotherapy of Cancer*, edited by R.M. Reilly (John Wiley & Sons, Inc., Hoboken, New Jersey, 2010).
6. D. Erickson, Riklund, K., Johansson, L., Stigbrand, T., "Radiation induced cell death", in *Targeted Radionuclide Therapy*, edited by T. Stigbrand, Carlsson, J., Adams, G.P. (Springer, 2008).
7. B. Brans, Bodei, L., Giammarile, F., et al., "Clinical radionuclide therapy dosimetry: the quest for the "Holy Gray", " *Eur J Nucl Med Mol Imaging* 34, 772-786 (2007).
8. M. G. Stabin, "Update: the case for patient-specific dosimetry in radionuclide therapy," *Cancer Biother Radiopharm* 23 (3), 273-284 (2008).
9. G.A. Wiseman, Kommehl, E., Leigh, B., et al., "Radiation dosimetry results and safety correlations from 90Y-Ibritumomab Tiuxetan radioimmunotherapy for relapsed or refractory non-Hodgkin's lymphoma: Combined data from 4 clinical trials," *J Nucl Med* 44 (3), 465-474 (2003).
10. S. Shen, Meredith, R.F., Duan, J., et al. , "Improved prediction of myelotoxicity using a patient-specific imaging dose estimate for non-marrow-targeting 90Y-antibody therapy," *J Nucl Med* 43 (9), 1245-1253 (2002).
11. S. Pauwels, Barone, R., Walrand, S., et al., "Practical dosimetry of peptide receptor radionuclide therapy with 90Y-labeled somatostatin analogs," *J Nucl Med* 46 (1), 92S-98S (2005).
12. A. Green, Flynn, A., Pedley, R.B., Dearling, J., Begent, R., "Nonuniform absorbed dose distribution in the kidney: The influence of organ architecture," *Cancer Biotherapy & Radiopharmaceuticals* 19 (3), 371-377 (2004).
13. M. Hough, Johnson, P., Rajon, D., et al., "An image-based skeletal dosimetry model for the ICRP reference adult male—internal electron sources," *Phy Med Biol* 56, 2309-2346 (2011).
14. J. F. Fowler, Stern, B.E., "Dose-rate effects: Some theoretical and practical considerations," *Brit J Rad* 33 (390), 389-395 (1960).
15. R. G. Dale, "The application of the linear-quadratic dose-effect equation to fractionated and protracted radiotherapy," *Br J Radiol* 58 (690), 515-528 (1985).
16. W. T. Millar, "Application of the linear-quadratic model with incomplete repair to radionuclide directed therapy," *Br J Radiol* 64 (759), 242-251 (1991).
17. A. R. Prideaux, H. Song, and R. F. Hobbs, et al., "Three-dimensional radiobiologic dosimetry: application of radiobiologic modeling to patient-specific 3-dimensional imaging-based internal dosimetry," *J Nucl Med* 48 (6), 1008-1016 (2007).

18. J. A. O'Donoghue, "Implications of nonuniform tumor doses for radioimmunotherapy," *J Nucl Med* 40, 1337-1341 (1999).
19. A.I. Kassis, Adelstein, S.J., "Radiobiologic principles in radionuclide therapy," *J Nucl Med* 46 (1), 4S-12S (2005).
20. B.G. Wouters, Sy, A.M., Skarsgard, L.D., "Low-dose hypersensitivity and increased radioresistance in a panel of human tumor cell lines with different radiosensitivity," *Radiation Research* 146, 399-413 (1996).
21. B. Marples, P. Lambin, K. A. Skov, and M. C. Joiner, "Low dose hyper-radiosensitivity and increased radioresistance in mammalian cells," *Int J Radiat Biol* 71 (6), 721-735 (1997).
22. B. Marples and S.J. Collis, "Low-dose hyper-radiosensitivity: Past, present, and future," *Int J Radiat Biol* 70 (5), 1310-1318 (2008).
23. L.A. Dawson, Kavanagh, B.D., Paulino, A.C., et al., "Radiation-associated kidney injury," *Int J Radiation Oncology Biol Phys* 76 (3), S108-S115 (2010).
24. B. Lambert, Cybulla, M., Weiner, S.M., Van De Wiele, C., Ham, H., Dierckx, A., Otte, A., "Renal Toxicity after Radionuclide Therapy," *Radiation Research* 161 (5), 607-611 (2004).
25. R. G. Dale, "Use of the Linear-Quadratic Radiobiological Model for Quantifying Kidney Response in Targeted Radiotherapy," *Cancer Biotherapy & Radiopharmaceuticals* 19 (3), 363-370 (2004).
26. L. Bodei, Cremonesi, M., Grana, C., et al., "Receptor radionuclide therapy with 90Y-[DOTA]0-Tyr3-octreotide (90Y-DOTATOC) in neuroendocrine tumours," *Eur J Nucl Med Mol Imaging* 31 (7), 1038-1046 (2004).
27. A.A. Flynn, Pedley, R.B., Green A.J., Dearling, J.L., El-Emir, E., Boxer, G.M., Boden, R., Begent, R.H.J., "The Nonuniformity of Antibody Distribution in the Kidney and its Influence on Dosimetry," *Radiation Research* 159 (2), 182-189 (2003).
28. R. Barone, Borson-Chazot, F., Valkema, R., et al., "Patient-specific dosimetry in predicting renal toxicity with 90Y-DOTATOC: relevance of kidney volume and dose-rate in finding a dose-effect relationship," *Journal of Nuclear Medicine* 46 (1), 99S-106S (2005).
29. B.W. Wessels, Konijnenberg, M.W., Dale, R.G., Breitz4, H.B., Cremonesi, M., Meredith R.F., Green, A.J., Bouchet, L.G., Brill, A.B., Bolch, W.E., Sgouros, G., and Thomas, S.R., "MIRD Pamphlet No. 20: The effect of model assumptions on kidney dosimetry and response—implications for radionuclide therapy," *Journal of Nuclear Medicine* 49 (11), 1884-1899 (2008).
30. J. O'Donoghue, "Relevance of external beam dose-response relationships to kidney toxicity associated with radionuclide therapy," *Cancer Biother Radiopharm* 19 (3), 378-387 (2004).
31. M. Cremonesi, Ferrari, M., Bodei, L., Tosi, G., Paganelli, G., "Dosimetry in peptideradionuclide receptor therapy: a review," *J Nucl Med* 47 (9), 1467-1475 (2006).
32. J.R. Cassady, "Clinical Radiation Nephropathy," *Int J Radiation Oncology Biol Phys* 31 (5), 1249-1256 (1995).
33. M. S. Kaminski, J. Estes, and K. R Zasadny, et al, "Radioimmunotherapy with iodine (131)I tositumomab for relapsed or refractory B-cell non-Hodgkin lymphoma: updated results and long-term follow-up of the University of Michigan experience," *Blood* 96 (4), 1259-1266 (2000).
34. Y.K. Dewaraja, Schipper, M. J., Roberson, P. L., Wilderman, S. J., Amro, H., Regan, D. D., and K. F. Koral, Kaminski, M. S., and Avram, A. M., "131I-Tositumomab Radioimmunotherapy: Initial Tumor Dose-Response Results Using 3-Dimensional Dosimetry Including Radiobiologic Modeling," *Journal of Nuclear Medicine* 51, 1155-1162 (2010).
35. H. Amro, S.J. Wilderman, Y. K. Dewaraja, and P. L. Roberson, "Methodology to incorporate biologically effective dose and equivalent uniform dose in patient-specific 3-dimensional dosimetry for Non_Hodgkin's Lymphoma patients targeted with 131I-tositumomab therapy," *J Nucl Med* 51 (4), 654-659 (2010).
36. P.L. Roberson, Amro, H., Wilderman, S.J., et al., "Bio-effect model applied to 131I radioimmunotherapy of refractory non-Hodgkin's lymphoma," *Eur J Nucl Med Mol Imaging* 38 (5), 874-883 (2011).